Propagation Modeling for Outdoor-to-Indoor and Indoor-to-Indoor Wireless Links in High-Speed Train

Lei Zhang[a,b,*], José Rodríguez-Piñeiro[c], Jean R. O. Fernández[b], José A. García-Naya[c], David W. Matolak[d], Cesar Briso[b], Luis Castedo[c]

[a] *Shanghai Institute of Microsystem and Information Technology, Chinese Academy of Sciences, Shanghai 200050, China*
[b] *Department of Signal Theory and Communications, Technical University of Madrid, 28031 Madrid Spain*
[c] *Department of Computer Engineering, University of A Coruña, 15071 A Coruña Spain.*
[d] *Department of Electrical Engineering, University of South Carolina, Columbia, SC 29208 USA*

Abstract

Nowadays telecommunication companies have shown a great interest in deploying broadband mobile wireless networks in high-speed trains (HSTs) with the aim of supporting both passenger services provisioning as well as automatic train control and signaling. The train carriage, as a confined steel structure, has specific propagation characteristics, which motivates the study of the indoor-to-indoor and outdoor-to-indoor radio propagation characteristics for broadband wireless communication systems in high-speed railways, constituting the main contribution of this work. This study has been performed by means of measurements considering an actual Long Term Evolution (LTE) network deployment, as well as a portable test transmitter and different configurations of antennas and receivers at 2.4, 2.6 and 5.7 GHz in a commercial high-speed rail line in Spain. The results show that radio waves incur obvious waveguiding effects inside the HST car. Moreover, for the propagation from the railway station to a mobile receiver inside the HST car, waves at higher frequencies experience less

*Corresponding author
Email addresses: lei.zhang@mail.sim.ac.cn (Lei Zhang), j.rpineiro@udc.es (José Rodríguez-Piñeiro), jean.raphael.olivier.fernandez@gmail.com (Jean R. O. Fernández), jagarcia@udc.es (José A. García-Naya), matolak@cec.sc.edu (David W. Matolak), cbriso@diac.upm.es (Cesar Briso), luis@udc.es (Luis Castedo)

attenuation through the train carriage, by better propagating through windows. Although the railway station and train interior contain objects that induce a rich set of multipath components, the analysis of small-scale fading statistics shows that the channel still has a dominant path. Also, the LTE coverage tests for Base Transceiver Station (BTS)-Train and BTS-Mobile links were conducted and with internal and external antennas on board the train. We found that there was a strong signal penetration loss of approximately 26 dB caused by the train carriage structure. The final results constitute an initial model for the propagation incurred by a relay-based communications system for fourth generation (4G) network in railways.

Keywords: Propagation measurements, channel modeling, railway, high speed train, relay system, LTE.

1. Introduction

During the last few years, the increasing demand for the use of mobile phones, laptops and other wireless devices by high-speed-train passengers has attracted great interest from railway companies. Simultaneously, the Mobile-Relay technique has been proposed in [1] as a way to provide coverage to passengers based on a relaying scheme (from cellular base to an external antenna on the train, which is then relayed to a local base within the train carriage).

These factors motivate the increasing interest in the radio propagation characteristics for wireless communication systems in railways, with the aim of providing broadband communications in trains [2]. Propagation properties for different yet related scenarios involving outdoor-to-indoor transmission with movement have been studied, such as for elevator shafts [3], cars [4], aircraft [5], indoor environments [6], such as rooms, corridors, and tunnels [7] [8]. In these settings, researchers concluded that path loss exponents are less than 2 in the confined scenarios, which indicate waveguiding effects. This effect also has been reported in [9], [10], and [11] in the case of radio propagation aboard the train in the 2 GHz band. Reflected waves from car-body in railway tunnel at 2.4 GHz

have been estimated by Finite-Difference Time-Domain (FDTD) analysis in [12], which states that a nearby train does not significantly affect the radio propagation. Experimental results in [13] have shown an extra 10.4 dB loss of the signal re-entering through the windows of the train in Inter-Car links at 5 GHz. The performance for fourth generation (4G) systems under high-speed conditions in a car by using both antennas placed outdoors and indoors was experimentally studied in [14], while in [15] a similar scheme was deployed for subway tunnel scenarios. Outdoor-to-indoor high speed channels were also evaluated by means of measurements and simulations in [16] and [17].

In general, a wireless network access system for the railway environment can be classified into five types:

1. Intra-Car link: the link between a mobile receiving device and an Access Point (AP), both located inside the same railway car.
2. Inter-Car link: the link between a mobile receiving device inside one railway car and the AP located inside another other railway car.
3. Station-Mobile link: the link between a mobile receiving device inside one railway car and the transmitter located in the railway station.
4. Base Transceiver Station (BTS)-Train link: the outdoor-to-outdoor link between a BTS and the external antennas of the train.
5. BTS-Mobile link: the outdoor-to-indoor link between a BTS and a mobile device inside the train.

The main contribution of this article is to present a propagation study for the five aforementioned wireless communication links by means of measurements in the real train environment at three frequencies: 2.4 GHz, 2.6 GHz and 5.7 GHz, which cover both the outdoor-to-indoor and indoor-to-indoor scenarios in railways. Different setups are considered to model both the large-scale and small-scale fading inside the train. On the other hand, the average SNR gain when using the outdoor antennas with respect to the indoor ones is about 26 dB for the whole path.

The rest of the paper is structured as follows: Section 2 describes the sce-

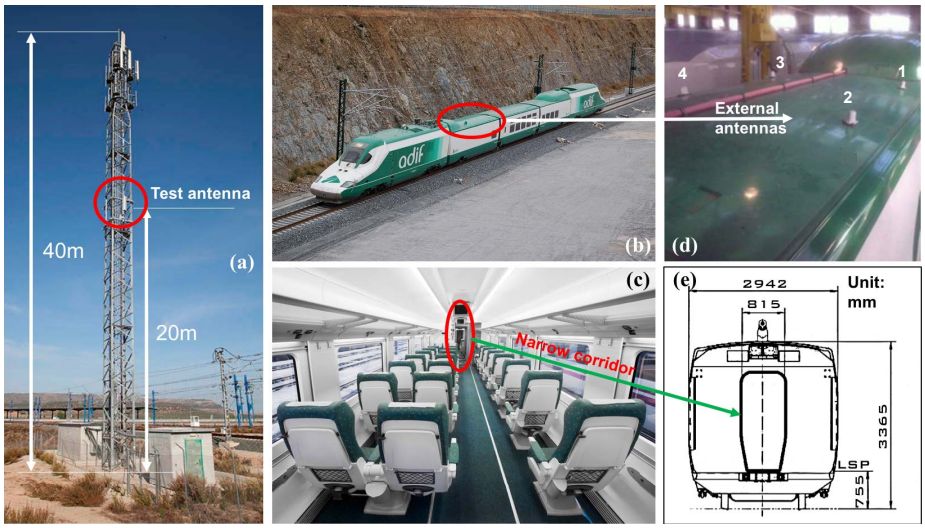

Figure 1: Measurement environment: (a) LTE BTS tower structure with the eNodeB 2.6 GHz antennas installed at a height of 20 m; (b) snapshot of the test train by Pablo Nieto, via: www.ferropedia.es; (c) interior of the commercial train car, via: www.talgo.com; (d) four external antennas on the roof of the train carriage; (e) cross section of the test train.

narios as well as the equipment used for the measurement campaign in the high-speed test line; Section 3 presents the empirical results, the path loss models for the wireless communication links and small scale fading evaluations, as well as the presentation and analysis of the results from broadband Long Term Evolution (LTE) signal measurements when the train is moving. Finally, Section 4 is devoted to the conclusions.

2. Experimental Setup

We evaluated experimentally the five types of wireless network access systems for the railway environments that we have considered: intra-car, inter-car, station-mobile, BTS-train, and BTS-mobile. Our aim is to compare the classical approach of direct communication link between the BTS and the mobile receiver of each passenger inside the train with an alternative approach based on a relay architecture where the signal is distributed inside the train through repeaters or APs, whereas external (train-car mounted) antennas are used for the BTS-train

link. It is worth noting that at least two different links are involved in a relay architecture, which are: (a) the BTS-train link, and (b) the Intra-Car link (or the Inter-Car link). In this work, these links are studied independently, e.g., no coordination or interference between these links is considered. In a practical deployment, several possibilities could be implemented, such as: (i) a simple amplify & forward scheme or (ii) each AP on the train acts as a femtocell to the LTE network [18]. Whereas the first approach is probably the simplest one, some interference management mechanism is required in case that the same frequency bands are used for both links in Frequency Division Duplex (FDD). Regarding the second approach, it may be more efficient in terms of resource sharing, although it would probably require the installation of a different femtocell per network operator. Alternatives involving non-LTE signals inside the train could be also considered, such as Wi-Fi APs.

The railway test environment described above is shown in Fig. 1, where the tower used for the BTS antenna deployment, the test train, and the interior of a train car are shown.

2.1. Measurement Environment

The measurement campaign was conducted at the high-speed rail line between Córdoba and Málaga (Spain), where the commercial operation speed reaches up to 330 km/h. The test track is a segment in the vicinity of Antequera-Santa Ana railway station (Kilometric Point (KP) 96.800). This track section includes a BTS site located at KP 97.075[1] consisting of 2G/3G commercial equipment with a 40 m height tower with antennas for different wireless technologies and frequencies (see Fig. 1(a)). The train was parked at the railway station (not moving) for the measurements considering intra-car, inter-car, and station-mobile links; and moving in the open area during the tests of BTS-train and BTS-mobile links.

[1]The exact Global Positioning System (GPS) coordinates of the site are 37° 4′ 3.14″ N, 4° 43′ 12.52″ W.

Figure 2: Photographs of: (a) transmitting system setup (only 2.4 and 5.7 GHz frequency bands are considered); (b) receiving system setup; (c) the surrounding environment of the railway station, via: http://turismoytren.com.

The test train was the *Séneca* laboratory train (Talgo A-330) provided by the Spanish railway operator ADIF. It is a 80.92 m long electric train that can reach a maximum speed of 363 km/h (see Figs. 1 (b) and (c)). The cross section of the *Séneca* train is shown in Fig. 1 (e), which also specifies the size of the narrow transition door between carriages.

2.2. Evaluated Wireless Network Access Systems

Two different testbeds were used to measure the five considered wireless network access systems. The first testbed is used for modeling the propagation conditions of a receiver inside the train carriages (intra-car, inter-car, and station-mobile link measurements), whereas the second one –the so-called GTEC Testbed [19]– is employed for measuring the propagation between the train and a commercial Evolved NodeB (eNodeB) when using external and internal antennas at the train (BTS-train and BTS-mobile link measurements, respectively).

2.2.1. Intra-Car, Inter-Car, and Station-Mobile Link Measurements

These measurements were performed with the train parked at the railway station. The propagation testbed transmitter was installed at a fixed position in the first car, whereas the testbed receiver was moved inside the train for the intra-car and inter-car links. For the station-mobile link, the transmitter was placed at the platform and the receiver was moved inside the train. The moving distance of the receiver is about 40 m, which is longer than the length of two train cars.

The propagation testbed transmitter consists of two continuous wave (CW) transmitters followed by power amplifiers and antennas for each considered carrier frequency (see Fig. 2 (a), the corresponding configuration parameters of the testbed are listed in Table 1). At the receiver, the testbed consists of a portable spectrum analyzer with a pre-amplifier as shown in Fig. 2 (b). The sensitivity is −100 dBm and the dynamic range is 100 dB, from 0 to −100 dBm. All these devices are controlled by a custom-developed software installed in a laptop computer. On the other hand, the two receive antennas for 2.4 GHz and 5.7 GHz are omnidirectional in azimuth, and they are connected to the receiver and attached on the shoulder of the operator at 1.6 m height, whereas the transmitter antenna height is 1.7 m. Note that measurements were carried out at both frequencies separately.

Table 1: Parameters of the testbed transmitter (EIRP stands for Effective Isotropic Radiated Power).

Frequency	Tx Power	Antenna Gain	EIRP
2.4 GHz	28.8 dBm	5 dBi	33.8 dBm
5.7 GHz	19.5 dBm	6.5 dBi	26 dBm

2.2.2. BTS-Train and BTS-Mobile Links

For these scenarios, the train moves at a constant speed of 50 km/h between KPs 93.4 and 102.0, passing in front of the tower where the eNodeB antennas are installed at KP 97.075. Note that measurements involving LTE BTS-train and BTS-mobile links are carried out simultaneously, thus the same transmitted LTE signals are acquired at the same time by the two indoor and the two outdoor antennas. A center frequency carrier of 2.6 GHz was used for the LTE measurements. The results of a LTE radio coverage study appear in Fig. 4, obtained by using the 9955 RNP (Radio Network Planning) tool from Alcatel-Lucent considering the same values for antenna orientation and transmit power as those employed in the measurements. The most relevant parameters are specified in Table 2.

Table 2: LTE testbed configuration parameters.

Parameter	Value
Transmit power	46 dBm
Carrier frequency	2.6 GHz
Bandwidth	10 MHz (9 MHz occupied)
Number of subcarriers	1024 (600 used)
LTE Transmission Mode	TM-2 (Transmit diversity) [20]*
Cyclic prefix length	Normal [21]**

*: A single transmit block is encoded and transmitted through two different antennas. Precoding is performed in order to separate the two different antennas [20].

**: The first OFDM symbol of an LTE slot (a slot occupies half a subframe) has a cyclic prefix length of 80 samples (5.2083 microseconds), whereas for the remaining six OFDM symbols the cyclic prefix is reduced to 72 samples (4.6875 microseconds) [21].

In this case we employed a commercial LTE eNodeB with two sectors deployed, referred to as the north and the south sector. The eNodeB was installed in one of the cabins of the BTS and two remote radio heads (each one connected

to two antenna elements in the same antenna panel) were mounted at the tower structure at a height of 20 m (see Fig. 1 (a)).

Both transmit antenna panels (Moyano MY-DTBSBS17276518) were oriented as the commercial GSM-R antennas already installed on the same tower. At the carrier frequency considered in the measurements, these cross-polarized antennas feature a gain of 18 dBi and half-power beam width of 62° (horizontal) and 5° (vertical). The antenna panel which serves the north sector has an azimuth orientation of 355° and a tilt of 0° (both electrical and mechanical), whereas the one radiating for the south sector has an azimuth orientation of 175° but a total tilt of −1.4° (0° mechanical and −1.4° electrical).

The LTE testbed receiver consists of two nodes from the GTEC Testbed (described in [22, 19]) operating in receive-only mode. Each node consists of a single USRP B210 board built from the Analog Devices AD9361 chip and a laptop computer with the so-called GTEC 5G Simulator [19]. Notice that the source code of both the GTEC Testbed and the GTEC 5G Simulator is publicly available under the GPLv3 license at `https://bitbucket.org/tomas_bolano/gtec_testbed_public.git`.

Both LTE testbed receiver nodes were installed inside the train (see Fig. 3). One of them (Fig. 3 (d)) was connected to two of the four antennas (more specifically, antenna number 1 and antenna number 2) available on the roof of the train carriage (Fig. 1(d)), which corresponds to the BTS-train link. The distance between the considered outdoor antennas is approximately 2 m. It is worth noting that there is a "hump" on the roof of the carriage (see Fig. 1(d)) which can partially block the signal for some of the receive antennas at some points of the train trajectory. The other receiver was connected to two of the four omni-directional antennas installed inside the carriage (Figs. 3 (c) and (e)), emulating a passenger mobile terminal directly attached to the LTE network (BTS-mobile link), thus enabling us to compare the signals captured by indoor and outdoor receivers. As seen in Figs. 3 (c) and (e), the indoor receive antennas are placed in front of a window which is located almost below the outdoor antenna number two. Additionally, each node was provided with a GPS receiver

Figure 3: LTE testbed receiver installed at the train carriage: (a) connection panel for the external antennas; (b) laptops of both testbed receiver nodes; (c) receiver node with its own indoor antennas (only two are used); (d) receiver node connected to the outdoor antennas (the additional attached antennas are just meant for test purposes); and (e) placement of the indoor antennas in the train carriage.

for geo-referencing (time and position) the measurements. Finally, Fig. 3 (a) shows the connection panel inside the train carriage, which allowed for the connection of the equipment to the external antennas mounted on the train roof.

3. Experimental Results

The empirical results obtained through the measurement campaign are presented in this section, both under static conditions as well as while the train

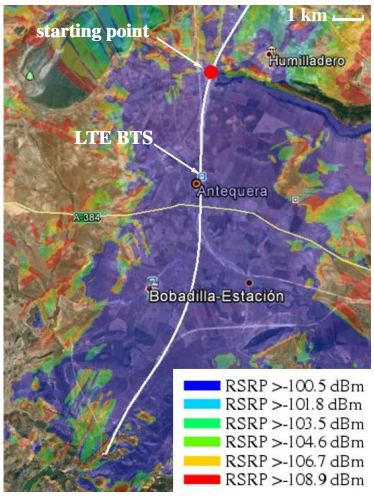

Figure 4: Simulation of the LTE radio coverage along the test track at 2.6 GHz. RSRP stands for Reference Signal Received Power, which is the average power received from the reference signal of a single LTE resource element.

was moving.

3.1. Intra-Car, Inter-Car, and Station-Mobile Links

The propagation inside the train at the carrier frequencies of 2.4 GHz and 5.7 GHz is measured in this paper. For this purpose, we assume that the LTE signal is distributed inside the train using repeaters or Wireless Local Area Network (WLAN) APs at these frequencies.

Fig. 5 shows the deployment considered for the measurements with transmitter and receiver on board. The testbed transmitter was installed on a seat of the first train carriage at a height of 1.7 m. The receiver was moved along the train corridor as indicated by the red arrow in Fig. 5, in which the normalized received power level is also plotted. It can be seen that the received power level increases slowly as the receiver moves toward the transmitter and reaches its peak value when the receiver passes by the transmitter. Then a large attenuation –more than 20 dB– is observed within the narrow corridor between carriages, because the inter-car door is noticeably narrower than the rest of the train structure (see Fig. 1 (e) and Fig. 5), thereby obstructing the received sig-

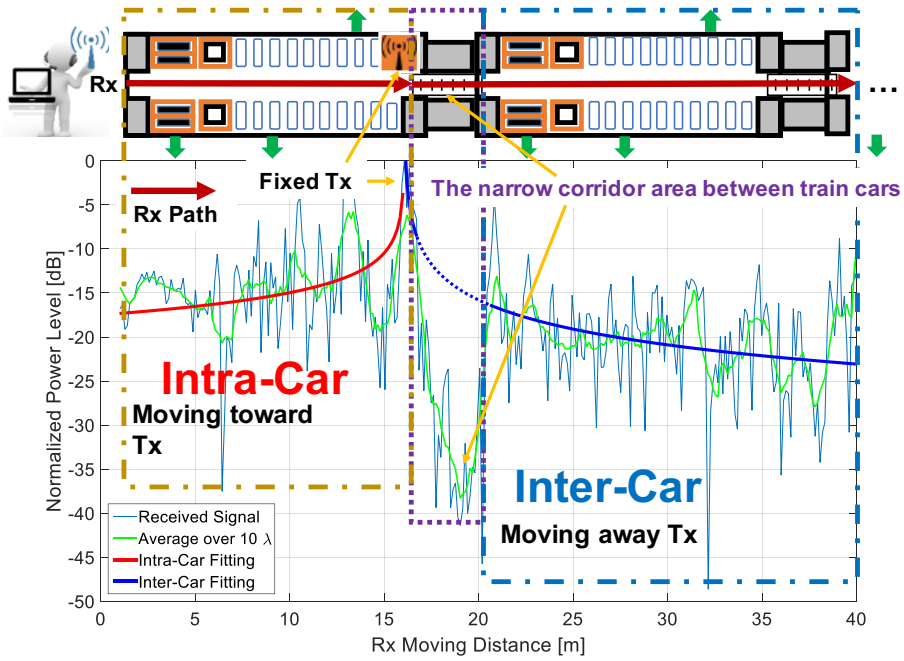

Figure 5: Received signal power level of the intra-car and inter-car links inside the *Séneca* train.

nal. This effect is also reported in [9] as a shielding loss of about 20 dB. When the operator arrives at the next train car, the multiple reflected waves from the surrounding environment (see Fig. 2 (c)) result in the power level rising back, but globally maintaining a downward trend as the receiver moves away the transmitter. Thus, the complete link can be divided into two parts based upon the location of the transmitter.

To model the attenuation and propagation in the case of an AP installed outside the train, e.g., on the platform of the railway station, corresponding measurements were conducted as illustrated in Fig. 6. In this case, the transmitter was placed in front of the second car and kept 3 m from the train door. The receiver was moved inside the train along the corridor of the first two cars. Then the operator moved outside and acquired the reference power level near the door and then re-entered the train. These measurements were repeated at both 2.4 GHz and 5.7 GHz.

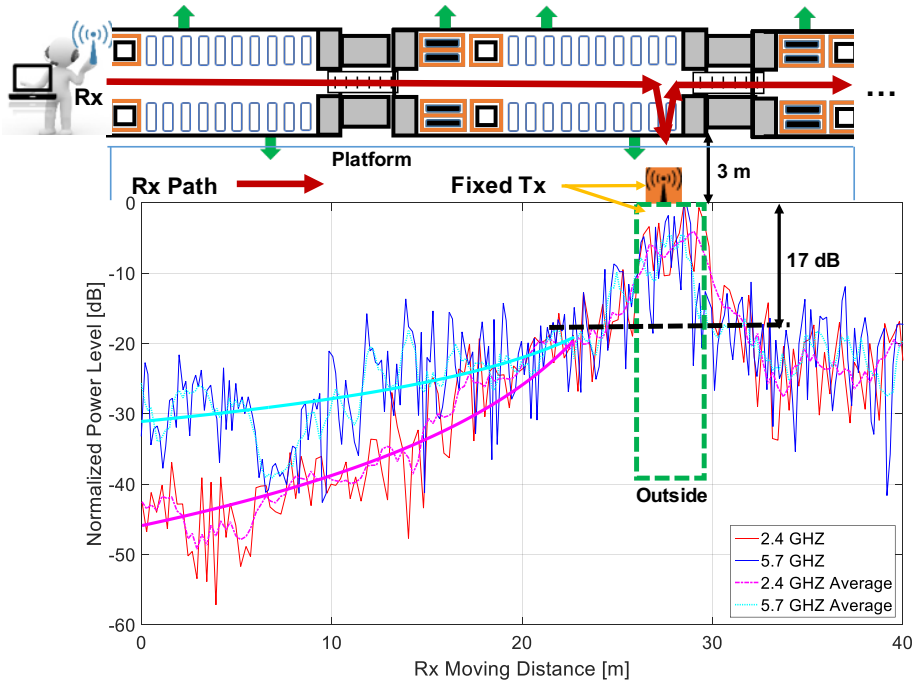

Figure 6: Received signal power level of station-mobile link at 2.4 GHz and 5.7 GHz.

The normalized received power level is also presented in Fig. 6. As the distance between transmitter and receiver decreases, the power level increases for both frequencies, especially after the operator moved out of the train. We notice an exemplary power level difference of ~ 17 dB from outside to inside. It is worth noting that propagation at 5.7 GHz experienced less attenuation than at 2.4 GHz. A similar conclusion can be found in [8].

Propagation is affected by the distance-dependent attenuation plus the large-scale shadowing and small-scale fading. The large-scale shadowing is the result of large obstructions, and the small-scale fading arises due to the constructive and destructive combination of multipath components. Thus, to separate the large-scale and small-scale fading, channel gain is averaged over ten wavelengths. For obtaining our propagation model inside the train, the narrow corridor with a large shielding loss is not considered during the fitting process as shown in Fig 5. The log-distance path loss model is used to predict the propagation loss

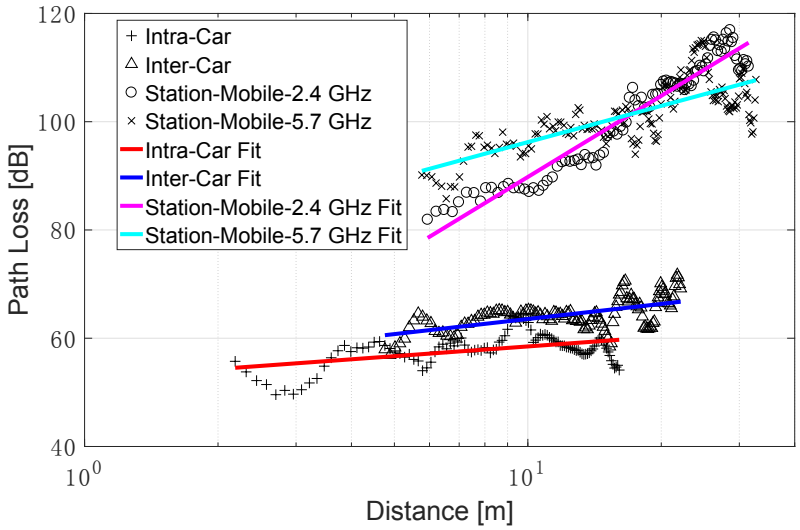

Figure 7: Path loss and least-square fittings for intra-car, inter-car, and station-mobile links.

for many applications. The path loss in decibels (dB) is found as the difference between transmitted power P_{Tx} and received power P_{Rx}, and the loss is modeled versus the logarithm of the distance as follows:

$$P_L(d) = P_{\mathrm{Tx}} - P_{\mathrm{Rx}} = P_0 + 10n \log_{10}\left(\frac{d}{d_0}\right) + X_s, \tag{1}$$

where d_0 is the close-in reference distance, P_0 is the fit intercept at d_0, and n is the path loss exponent, which describes the path loss trend with respect to the link distance d. X_s represents a zero mean Gaussian random variable expressed in decibels and with a standard deviation σ_x.

Through least-squares regression analysis, as presented in Fig. 7, the path loss exponents and their variations can be obtained. The path loss exponent n and the standard deviation σ_x of the variations in intra-car and inter-car links are listed in Table 3. It can be useful to compare these values to measurement results in similar scenarios, such as tunnels, halls, indoor corridors, and propagation from outdoor-to-indoor settings, as shown in Table 3. The path loss exponent n in free space is equal to 2. However, n is less than 2 in both the intra-car and inter-car links, which is similar to the cases of tunnels and corri-

Table 3: Path loss models for different environments including intra-car, inter-car and station-mobile links.

Scenario	Frequency	n	σ_x [dB]
Intra-Car	2.4 GHz	0.60	2.59
Inter-Car	2.4 GHz	0.93	2.34
Station-Mobile	2.4 GHz	3.81	2.93
	5.7 GHz	1.74	3.85
Intra-Car [9]	2.2 GHz	≈1.2	–
Aboard train [10]	2.45 GHz	1.71	≈2.33
Subway tunnel [7]	2.65 GHz	1.94	5.47
Indoor corridor [6]	5.25 GHz	1.8	3.10
Large indoor hall [6]	2-6 GHz	1.39-3.78	3-4

dors. These kinds of confined environments always produce a guiding effect on the signal, yielding an exponent less than 2. Furthermore, our n is smaller than the values typically obtained from corridors and subway tunnels. This is because the steel body of the train has a higher reflectivity than brick or concrete walls, and this strengthens the waveguide effect. The relatively small exponents have been observed in [9] and [10] on board the train, but our smaller n is due to the presence of more metallic equipments and more crowed inner space. Next, the n larger in the inter-car link than in the intra-car link predicts a higher path loss in the following train cars because of the changes in the train structure.

When the transmitter is located outside the train, the transmitted waves penetrate the train car body and continue their propagation inside the train. Thus the propagation is partially affected by the waveguide effect. As waveguide theory shows, waves at higher frequencies experience smaller propagation losses [8]. Thus, n is larger at 2.4 GHz than at 5.7 GHz.

In the case of the station-mobile link it is also a *semi confined* environment as shown in Fig. 2 (c). When the train is at the platform there is a steel structure covering the platform, hence confined propagation is possible although

we have measured important differences between 2.4 and 5.7 GHz path losses. This difference is due to the influence of the train windows, which increase losses at lower frequencies. This also explains why the observed losses at 2.4 GHz are much higher ($n = 3.84$).

For selecting the best fitting model to describe the small-scale fading, Akaike's Information Criteria (AIC) is introduced in [23]. AIC is a goodness of fit measure that favors smaller residual error in the model. The general form for calculating AIC is as follows:

$$\mathrm{AIC} = -2\log\left(\mathcal{L}\right) + 2U, \tag{2}$$

where $\log(\cdot)$ is the natural logarithm, $\mathcal{L}$ is the likelihood function of the associated distribution, and U is the number of free parameters in the model [24]. AIC scores are often evaluated by the AIC difference defined as

$$\Delta\mathrm{AIC}_j = \mathrm{AIC}_j - \min_i\left(\mathrm{AIC}_i\right), \tag{3}$$

where $\min_i\left(\mathrm{AIC}_i\right)$ is the minimum AIC over $i = 1, \ldots, J$ distribution models. So the best model has a ΔAIC equal to 0. Furthermore, the Akaike weights can be introduced as conditional probabilities for each mode, and greatly facilitating the comparisons among the candidate models [25]. The j-th Akaike weight w_j is given by:

$$w_j \;=\; \frac{\exp\left\{-\frac{1}{2}\Delta\mathrm{AIC}_j\right\}}{\sum_{i=1}^{J}\exp\left\{-\frac{1}{2}\Delta\mathrm{AIC}_i\right\}}, \tag{4}$$

where $\sum_{j=1}^{J} w_j = 1$. Akaike weights provide a straightforward interpretation based on the probability of each model to become the best model in an AIC sense. Therefore, the model with the highest Akaike weights is usually the preferred one.

For small-scale fading, although Rayleigh and Rician distributions have been proposed and performed well in describing multipath fading statistics in many cases, other models, such as the Nakagami and Weibull distributions, are considered as generalized alternative solutions. These distributions include Rayleigh as a special case and can be more accurate in matching some experimental data [26, 27]. Thus, we fit the received signal amplitudes (large-scale fading

Table 4: Akaike weights of the four distribution candidates, and the fitting shape factors of Nakagami and Weibull distributions.

Link	Frequency	Rayleigh	Rician	Nakagami	Weibull	Shape factors [m; β]
Intra-Car	2.4 GHz	0.0193	0.0430	0.8014	0.1362	[1.50; 2.39]
Inter-Car	2.4 GHz	0.0928	0.1447	0.4836	0.2789	[1.30; 2.30]
Station-	2.4 GHz	0.0442	0.0862	0.6214	0.2481	[1.44; 2.41]
Mobile	5.7 GHz	0.1492	0.0549	0.6234	0.1725	[1.25; 2.19]

removed) with these four empirical distributions: Rayleigh, Rician, Nakagami, and Weibull. The Akaike weights of these distribution models are listed in Table 4. Results clearly show that the Nakagami is the best fit model with the highest Akaike weights for all links, whereas the Weibull is the second best. Note that the shape factors m of Nakagami and β of Weibull are also provided in Table 4. Fig. 8 shows the plot of the empirical Cumulative Distribution Functions (CDFs) against the CDFs of the Nakagami distribution. In the special case $m = 1$ or $\beta = 2$, Rayleigh fading pertains, which implies the signal offered to the receiver does not contain a dominant wave. Whereas in our case, m and β are greater than 1 and 2, respectively. The Rayleigh distribution has the lowest Akaike weights in all links. As one would expect, even though there are rich reflection and scattering components inside the railway station and train car, the fading in the intra-car, inter-car, and station-mobile links is not as severe as in a Rayleigh channel, and it can be described as a propagation channel with a dominant component.

Additionally, the multiple reflected waves outside the train can re-enter through the windows and thus leading to a reduction in the path loss compared with the case of a train outside in an open area. As the authors in [13] state, if the windows are covered with absorbers, there can be an additional 10.4 dB of path loss at 5.2 GHz. In our case, the windows are made out of heat-protective

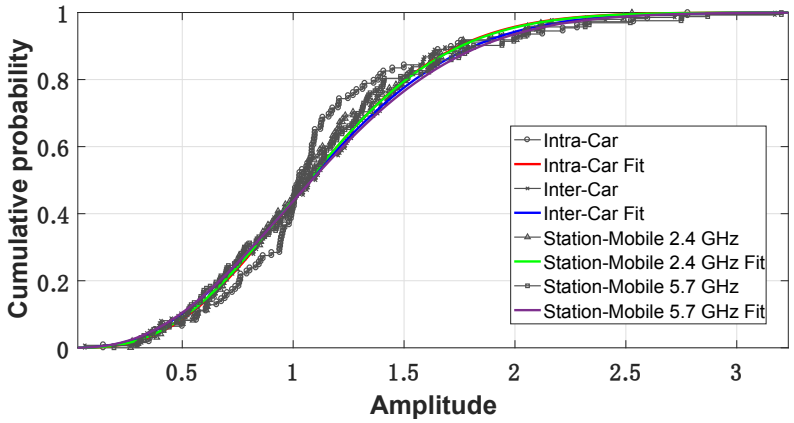

Figure 8: Fitting CDF of the small-scale fading with Nakagami distribution.

glass and covered by an absorber layer to attenuate sun light, and this layer can also attenuate wireless communication signals. There was a total attenuation of 40 dB imparted to the re-entering signals as described in [28]. This report assumed that fast moving scatterers outside the train do not considerably affect the propagation. The extra loss due to the windows may be different for different trains and different environments in which the train is operated, hence inducing a different amount of wave *re-entering*. However, these are topics for future research.

3.2. LTE for BTS-Train and BTS-Mobile Links

In this section, using the GTEC Testbed, we provide an empirical study of the estimated Signal-to-Noise Ratio (SNR) along the track surrounding the eNodeB when transmitting LTE signals as described in Section 2.2.2. The eNodeB (LTE transmitter) provides coverage for two different sectors while both receivers perform a handover approximately when the train passes in front of the tower where the eNodeB antennas are installed (see Table 2 and Fig. 4).

The SNR is estimated considering exclusively the data subcarriers. Thus, guard subcarriers, Direct Current (DC) subcarrier as well as pilot subcarriers are discarded *a priori*. However, for some cases the receiver is not able to correctly

detect an acquired LTE frame. In those cases the procedure is identical but the pilot subcarriers are not discarded since their positions on the time-frequency grid are unknown. This fact should not impact on the results significantly since no pilot power boosting was considered[2]. The SNR is estimated as follows:

1. Noise samples in the time domain are captured with the transmitter switched off (hence not transmitting any signal).
2. The captured noise samples in the time domain are then processed as if they were actual data samples, i.e., the cyclic prefix is removed, a Fast Fourier Transform (FFT) is performed and both guard and DC subcarriers are removed. Note that the noise samples corresponding to pilot subcarriers are only used when an LTE frame is not detected.
3. As a result, $w^{(b,k)}$ noise samples are obtained in the frequency domain, each one corresponding to the b-th subcarrier of the k-th Orthogonal Frequency-Division Multiplexing (OFDM) symbol, where $b \in \mathcal{D}^{(k)}$, being $\mathcal{D}^{(k)}$ the set of indexes of the data subcarriers (or the set of indexes of the data subcarriers plus the pilot subcarriers when the corresponding LTE frame is not detected) for the k-th OFDM symbol.
4. All the previous steps are repeated when the transmitter is switched on, hence $r^{(b,k)}$ data samples (of course also affected by noise) are obtained in the frequency domain.
5. The average SNR for the k-th OFDM symbol is then estimated by averaging out the instantaneous SNR values for the selected subcarriers. Defining

$$P_{r^{(k)}} = \frac{1}{\left|\mathcal{D}^{(k)}\right|} \sum_{b \in \mathcal{D}^{(k)}} \left| r^{(b,k)} \right|^2, \tag{5}$$

and

$$P_{w^{(k)}} = \frac{1}{\left|\mathcal{D}^{(k)}\right|} \sum_{b \in \mathcal{D}^{(k)}} \left| w^{(b,k)} \right|^2, \tag{6}$$

where $\left|\mathcal{D}^{(k)}\right|$ is the number of selected subcarriers for the k-th symbol.

[2]Both pilot and data symbols are transmitted with the same power.

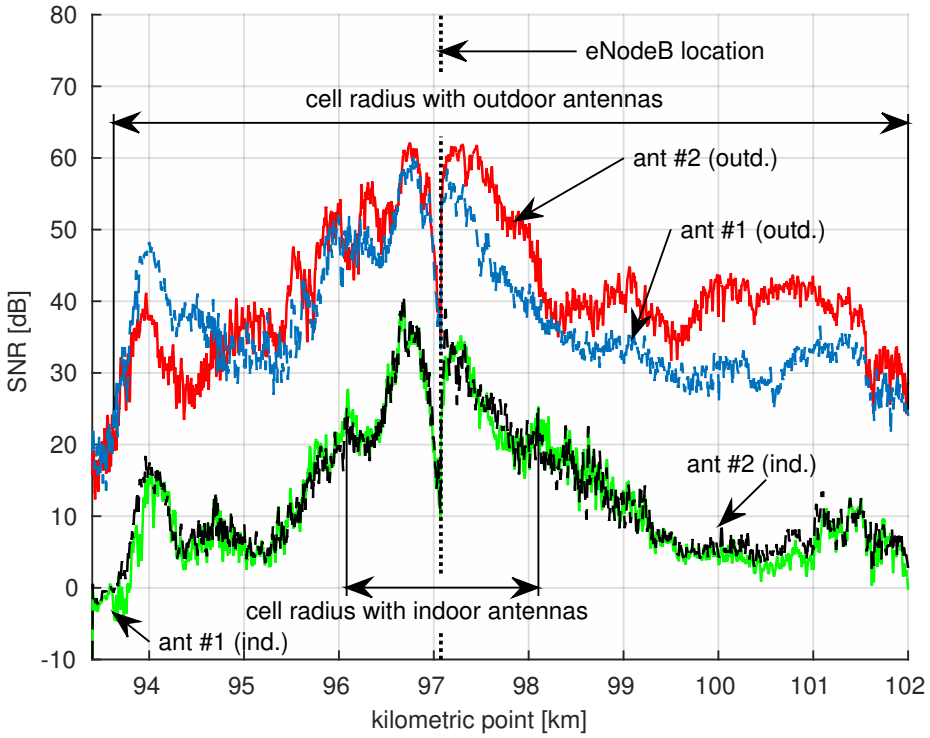

Figure 9: Estimated SNR values by means of measurements corresponding to both BTS-train and BTS-mobile links.

Then, the SNR for the k-th OFDM symbol is calculated as

$$\mathrm{SNR}^{(k)} = \frac{P_{r^{(k)}} - P_{w^{(k)}}}{P_{w^{(k)}}}. \tag{7}$$

Fig. 9 shows the estimated SNR values when the train moves between KPs 93.4 and 102.0 at 50 km/h. Four curves are included in each plot, two of them corresponding to two outdoor antennas located on the roof of the train carriage (namely "ant #1 (outd.)" and "ant #2 (outd.)") and the other two corresponding to the two indoor antennas (namely "ant #1 (ind.)" and "ant #2 (ind.)"). The horizontal axis in Fig. 9 shows kilometric point, while the vertical one shows the estimated SNR values in dB. The train carriage, where the receivers are installed, passes in front of the tower where the eNodeB antennas are installed at approximately KP 97.075 km. At this point, the handover between

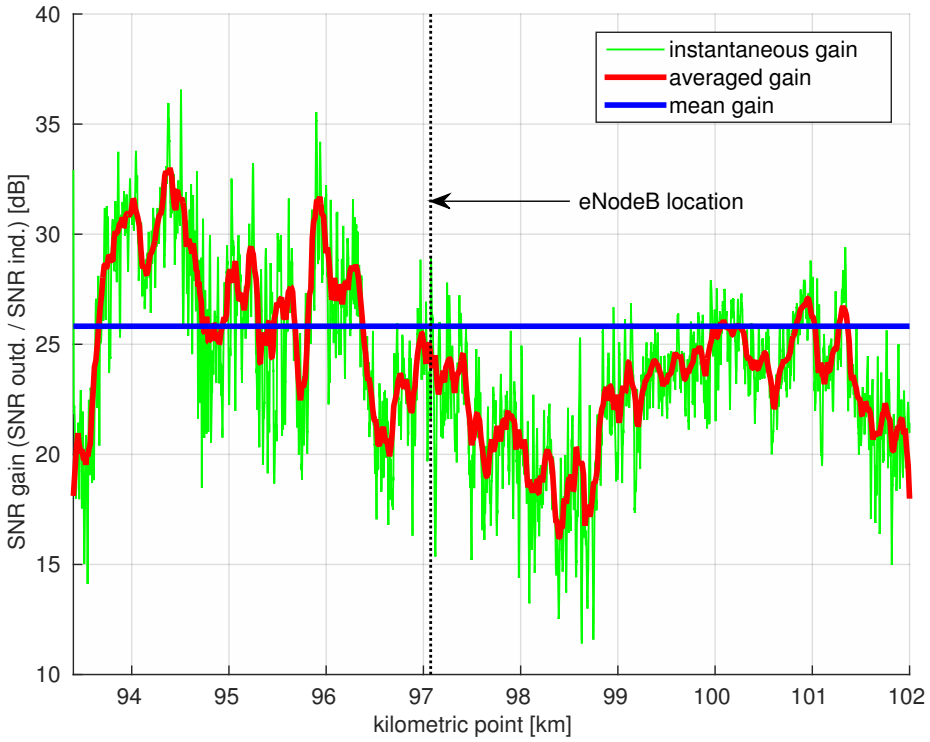

Figure 10: Estimated SNR difference between the BTS-external antenna and BTS-internal antenna.

the two deployed sectors occurs.

In Fig. 9 we can see that the obtained results are very similar for both outdoor antennas. The shape of the SNR curves corresponding to the indoor ones is also similar, but the SNR is reduced by approximately 26 dB due to the attenuation of the train car itself. It can be seen that the SNR values for the antennas placed outdoors are above 10 dB for all the considered measurement points, and the maximum values are obtained when the train is close proximity to the eNodeB antennas. The so-called cell radius is defined both for the outdoors and indoors antennas. We define the cell radius as the zone where the SNR is higher than a certain value. If such a value is set to 25 dB, for example, then it can be observed that the cell radius for the outdoor antennas is four times larger than for the indoor ones.

Fig. 10 shows more clearly the SNR gain between one of the outdoor antennas (namely "ant #1 (outd.)) and one of the indoor ones (namely "ant #1 (ind.)"). This SNR gain is computed as the difference between the instantaneous SNR values obtained for the outdoor antenna and the indoor one, both expressed in dBs. A curve obtained by averaging the instantaneous values by using a sliding window of 6.5 ms long is also included. It can be seen that, during most of the time, the SNR gain is between 20 dB and 35 dB. The average SNR gain for the whole path is also indicated in Fig. 10 and it is about 26 dB.

4. Conclusions

The main conclusions of this work are summarized as follows:

- As path loss models for the propagation inside the train reveal, intra-car and inter-car links at 2.4 GHz, and station-mobile links at 5.7 GHz are influenced by waveguiding effects, which result in path loss exponents less than 2. Attenuation along the train is lower than that of free space except for the narrow corridor between the carriages. Received signal amplitudes show good fittings with Nakagami-m and Weibull distributions with $m > 1$ and $\beta > 2$, respectively. This implies the presence of a dominant component for the intra-car, inter-car, and station-mobile links.

- The train carriage structure introduces a strong signal penetration loss. The amount of penetration loss was grossly estimated both by evaluating the difference between BTS-mobile and the BTS-train links via a standard-compliant LTE signal received by a moving train. For LTE signals received inside the train, the average attenuation observed with the train in movement was approximately 26 dB at 2.6 GHz. This large attenuation reduces the cell radius from 8.5 km with external antennas to 2 km with internal antennas.

Hence, to provide a reliable communication systems for HST passengers with reasonable cell sizes, it is necessary to employ a relay based solution with exter-

nal antennas. The signal inside the train cars can be easily distributed by using Wi-Fi access points or directly using repeaters.

Acknowledgements

This work has been developed under the framework of ENABLING 5G TEC2014-55735-C3-2-R funded by the Spanish Ministry of Economy and Competitiveness. This work has been also funded by the Xunta de Galicia (ED431C 2016-045, ED341D R2016/012, ED431G/01), the Agencia Estatal de Investigacin of Spain (TEC2013-47141-C4-1-R, TEC2015-69648-REDC, TEC2016-75067-C4-1-R) and ERDF funds of the EU (AEI/FEDER, UE). Financial support of the China Scholarship Council (CSC) research fellowship given to Lei Zhang is also acknowledged.

[1] 3GPP, Technical specification group radio access network; mobile relay for E-UTRA, Tech. Rep. 3GPP TR 36.836 (2012).

[2] C. Briso-Rodríguez, C. F. López, J. R. Fernández, S. Pérez, D. Draskovic, J. Calle-Sánchez, M. Molina, J. I. Alomso, C. Rodríguez, C. Hernández, J. Moreno, J. Rodríguez-Piñeiro, J. A. García-Naya, L. Castedo, Broadband Access in Complex Environment: LTE on Railway, IEICE Transactions on Communications 97 (8) (2014) 1514–1527, special Section on EU's FP7 R&D Project Activities on Future Broadband Access Technologies. Online access: `http://dx.doi.org/10.1587/transcom.E97.B.1514`.

[3] D. W. Matolak, R. Sun, Channel characteristics for elevator shafts at 5 GHz, in: Proc. of IEEE Global Communications Conference (GLOBECOM 2013), IEEE, 2013, pp. 3931–3935.

[4] F. Harrysson, J. Medbo, T. Hult, F. Tufvesson, Experimental investigation of the directional outdoor-to-in-car propagation channel, IEEE Transactions on Vehicular Technology 62 (6) (2013) 2532–2543.

[5] T. N. Moraitis, P. Constantinou, F. P. Fontan, P. Valtr, Propagation measurements inside different civil aircrafts and comparison with EM techniques, in: Proc. of 3rd European Conference on Antennas and Propagation (EuCAP 2009), IEEE, 2009, pp. 887–891.

[6] J. Meinilä, P. Kyösti, L. Hentilä, T. Jämsä, E. Suikkanen, E. Kunnari, M. Narandzic, D5. 3: Winner+ final channel models, Wireless World Initiative New Radio WINNER.

[7] M.-S. Choi, D.-Y. Kim, H.-S. Jo, J.-G. Yook, H.-K. Park, Path-loss characteristics in subway tunnels at 2.65 GHz, Microwave and optical technology letters 48 (2) (2006) 383–386.

[8] K. Guan, B. Ai, Z. Zhong, C. F. López, L. Zhang, C. Briso-Rodríguez, A. Hrovat, B. Zhang, R. He, T. Tang, Measurements and analysis of large-scale fading characteristics in curved subway tunnels at 920 MHz, 2400 MHz, and 5705 MHz, IEEE Transactions on Intelligent Transportation Systems 16 (5) (2015) 2393–2405. doi:10.1109/TITS.2015.2404851.

[9] N. Kita, T. Ito, S. Yokoyama, M. C. Tseng, Y. Sagawa, M. Ogasawara, M. Nakatsugawa, Experimental study of propagation characteristics for wireless communications in high-speed train cars, in: 2009 3rd European Conference on Antennas and Propagation, 2009, pp. 897–901.

[10] A. Mariscotti, A. Marrese, N. Pasquino, R. Schiano Lo Moriello, Characterization of the radio propagation channel aboard trains for optimal coverage at 2.45 GHz, in: Proc. of IEEE International Workshop on Measurements and Networking Proceedings (M&N 2013), IEEE, 2013, pp. 195–199.

[11] W. Dong, G. Liu, L. Yu, H. Ding, L. Zhang, Channel properties of indoor part for high-speed train based on wideband channel measurement, in: Proc. of 5th International ICST Conference on Communications and Networking in China (CHINACOM 2010), IEEE, 2010, pp. 1–4.

[12] M. Shirafune, T. Hikage, T. Nojima, M. Sasaki, W. Yamada, T. Sugiyama, Propagation characteristic estimations of 2 GHz inter-car wireless links in high-speed train cars in a railway tunnel, in: Proc. of International Symposium on Antennas and Propagation (ISAP 2014), IEEE, 2014, pp. 215–216.

[13] T. Ito, N. Kita, W. Yamada, M.-C. Tseng, Y. Sagawa, M. Ogasawara, M. Nakatsugawa, T. Sugiyama, Study of propagation model and fading characteristics for wireless relay system between long-haul train cars, in: Proc. of the 5th European Conference on Antennas and Propagation (EUCAP 2011), IEEE, 2011, pp. 2047–2051.

[14] P. Suárez-Casal, J. Rodríguez-Piñeiro, J. A. García-Naya, L. Castedo, Experimental evaluation of the WiMAX downlink physical layer in high-mobility scenarios, EURASIP Journal on Wireless Communications and Networking 2015 (109). doi:10.1186/s13638-015-0339-9.

[15] L. Zhang, P. Suárez-Casal, J. Fernandez, J. Rodríguez-Piñeiro, J. Calle-Sánchez, J. A. Garcia-Naya, L. Castedo, C. Rodríguez-Sánchez, J. Moreno, C. Briso-Rodríguez, J. Alonso-Montes, Experimental evaluation of 4G technologies in metro tunnel scenarios, in: Proc. of the 10th European Conference on Antennas and Propagation (EuCAP 2016), Davos, Switzerland, 2016, pp. 1–5. doi:10.1109/EuCAP.2016.7481740.

[16] J. Rodríguez-Piñeiro, M. Lerch, J. A. García-Naya, S. Caban, M. Rupp, L. Castedo, Emulating extreme velocities of mobile LTE receivers in the downlink, EURASIP Journal on Wireless Communications and Networking 2015 (106). doi:10.1186/s13638-015-0343-0.

[17] J. Rodríguez-Piñeiro, P. Suárez-Casal, M. Lerch, S. Caban, J. A. Garcia-Naya, L. Castedo, M. Rupp, LTE downlink performance in high speed trains, in: Proc. of 2015 IEEE 81st Vehicular Technology Conference (VTC2015-Spring), Glasgow, United Kingdom, 2015, pp. 1–5. doi:10.1109/VTCSpring.2015.7145924.

[18] L. Chen, Y. Huang, F. Xie, Y. Gao, L. Chu, H. He, Y. Li, F. Liang, Y. Yuan, Mobile relay in lte-advanced systems, IEEE Communications Magazine 51 (11) (2013) 144–151. doi:10.1109/MCOM.2013.6658666.

[19] T. Domínguez-Bolaño, J. Rodríguez-Piñeiro, J. A. Garcia-Naya, L. Castedo, The GTEC 5G link-level simulator, in: Proc. of the 1st International Workshop on Link- and System Level Simulations (IWSLS2 2016), Vienna, Austria, 2016, pp. 64–69. doi:10.1109/IWSLS.2016.7801585.

[20] ETSI, TS 136 213 V14.2.0: LTE; E-UTRA; Physical layer procedures (April 2017).

[21] ETSI, TS 136 211 V14.2.0: LTE; E-UTRA; Physical channel and modulation (April 2017).

[22] J. Rodríguez-Piñeiro, J. A. García-Naya, A. Carro-Lagoa, L. Castedo, A Testbed for Evaluating LTE in High-Speed Trains, in: Proc. of 16th Euromicro Conference on Digital System Design (DSD 2013), 2013, pp. 175–182, online access: http://dx.doi.org/10.1109/DSD.2013.27.

[23] R. He, Z. Zhong, B. Ai, J. Ding, Y. Yang, A. F. Molisch, Short-term fading behavior in high-speed railway cutting scenario: Measurements, analysis, and statistical models, IEEE Transactions on Antennas and Propagation 61 (4) (2013) 2209–2222. doi:10.1109/TAP.2012.2235399.

[24] K. P. Burnham, D. R. Anderson, Multimodel interference understanding AIC and BIC in model selection, Sociological methods & research 33 (2) (2004) 261–304.

[25] E.-J. Wagenmakers, S. Farrell, Aic model selection using akaike weights, Psychonomic bulletin & review 11 (1) (2004) 192–196.

[26] H. Suzuki, A statistical model for urban radio propogation, IEEE Transactions on Communications 25 (7) (1977) 673–680.

[27] I. Sen, D. W. Matolak, W. Xiong, Wireless channels that exhibit "worse than Rayleigh" fading: Analytical and measurement results, in: MILCOM 2006 - 2006 IEEE Military Communications conference, 2006, pp. 1–7. doi:10.1109/MILCOM.2006.302519.

[28] P. Kyösti, J. Meinilä, L. Hentilä, X. Zhao, T. Jämsä, C. Schneider, M. Narandžić, M. Milojević, A. Hong, J. Ylitalo, et al., Ist-4-027756 winner ii deliverable 1.1. 2. v. 1.2, winner ii channel models, IST-WINNER2, Tech. Rep.